Contemporary Mathematics
https://ojs.wiserpub.com/index.php/CM/

Research Article

Significance of Thermal Radiation in Heat Transfer of MHD Blood Based CNTs Hybrid Nanofluids Past a Stretching/Shrinking Sheet: A Couple-Stress Fluid Model

T. Alzkari[1], Ali Rehman[2], A. B. Albidah[1], Ilyas Khan[1,3,4,5,6*], N. F. M. Noor[7], K. Sudarmozhi[2], Wei Sin Koh[8]

[1] Department of Mathematics, College of Science Al-Zulfi, Majmaah University, Al-Majmaah 11952, Saudi Arabia
[2] Department of Mathematics, Saveetha School of Engineering, SIMATS, Chennai, Tamil Nadu, India
[3] Department of Mathematical Sciences, Saveetha School of Engineering, SIMATS, Chennai, Tamil Nadu, India
[4] Hourani Center for Applied Scientific Research, Al-Ahliyya Amman University, Amman, Jordan
[5] Irfan Gunsel Operational Research Institute in Healthcare, Near East University, Mersin 10, Nicosia, TRNC, Turkey
[6] Faculty of Art and Science, University of Kyrenia, Mersin 10, Nicosia, TRNC, Turkey
[7] Institute of Mathematical Sciences, Faculty of Science, Universiti Malaya, Kuala Lumpur 50603, Malaysia
[8] INTI International University, Persiaran Perdana BBN Putra Nilai, Nilai, Negeri Sembilan 71800, Malaysia
E-mail: i.said@mu.edu.sa

Received: 7 November 2025; **Revised:** 5 December 2025; **Accepted:** 30 December 2025

Abstract: The effect of thermal radiation on heat transport in a steady, two-dimensional blood-based nanofluid is studied. Blood is the base fluid with Multiwalled Carbon Nanotubes (MWCNT) and Single-Walled Carbon Nanotubes (SWCNT) nanoparticles. Blood flow is described with the couple-stress fluid model. Thermal radiation, couple stress effects, and viscous dissipation effects are considered, and the governing partial differential equations are transformed with similarity transformations, resulting in nonlinear ordinary differential equations, which are solved analytically with the Homotopy Analysis Method (HAM). The results investigated the velocity and temperature profiles, as well as the skin-friction and Nusselt-number distributions, across the shrinking/stretching sheet. The thermal radiation parameter was found to improve the Nusselt number by about 15%, improving the heat transfer rate. The couple stress parameters were found to reduce skin friction and strengthen the boundary layer. The heat transfer rate increased with a higher nanoparticle volume fraction, and SWCNTs resulted in a 42% increase in the Nusselt number compared to the blood-based fluid. The results are valuable in biomedical applications, especially in hyperthermia-based thermal therapy and drug delivery systems, in devices with high thermal regulation, such as artificial hearts and hemodialysis, and in thermal regulation devices.

***Keywords*:** thermal radiation, shrinking/stretching, Carbon Nanotubes (CNTs), Homotopy Analysis Method (HAM), couple stress, smart grid

MSC: 80A20, 76A05, 76D05

Copyright ©2026 Ilyas Khan, et al.
DOI: https://doi.org/10.37256/cm.7320269107
This is an open-access article distributed under a CC BY license
(Creative Commons Attribution 4.0 International License)
https://creativecommons.org/licenses/by/4.0/

1. Introduction

Nanofluids are thermal and physical property-enhanced fluids containing engineered colloidal suspensions of nanoparticles, typically less than 100 nm, in a base fluid. The fluids are of particular interest because their heat transfer capabilities exceed those of conventional fluids such as water and ethylene glycol. Hybrid nanofluids have further advanced the concept by using two or more different types of nanoparticles in a base fluid, resulting in improved thermal conductivity, heat transfer, and overall system stability compared to mono nanofluids. The protective response of matrix-coated particles, which consist of a nanolayer of particles and are in the less-thermally-conductive centre of a fluid, to the heat contact with the surrounding fluid serves to improve critical thermal characteristics of the fluid to enhance the fluid's inner flow capabilities to positively respond to heat transfer demands of advanced thermal management applications.

To optimize the properties of base fluids and nanoparticles for various technological applications, researchers are continuously investigating novel combinations in nanofluids, including hybrid nanofluids. Shahzadi et al. [1] studied blood flow in hybrid nanofluids through bifurcated stenosed arteries, which are strongly affected by permeability. Ellahi et al. [2] examined the blood flow of nanofluids via an artery with composite stenosis and porous walls. Dinarvand et al. [3] examined how to enhance the microcirculatory drug delivery system by using a hybrid nanofluid flow pattern along a permeable, stretched surface. Chahregh et al. [4] investigated the flow of a TiO_2-Ag/blood hybrid nanofluid through an artery, with applications to medication administration and blood circulation in the respiratory system.

The study of flow and heat transfer at stretching and shrinking surfaces is instrumental to processes like the cooling of stretching sheets, polymer extrusion, and continuous casting. The heat and fluid dynamics of flow and thermal contact with the interface's surface is of primary interest because the boundary layer characteristics and transfer rates of heat vary depending on whether the surface is stationary or moving, especially in opposite directions. The thermal contact and shear forces of the surfaces of the enclosed systems are critical to the processes and devices of an engineered process or system.

Misra et al. [5] investigated the impact of coupled stressors on the blood's electrokinetic oscillatory flow within the microcirculatory system. Kollin et al. [6] investigated the method's foundation and its application to measuring blood flow. Korchevskii et al. [7] investigated the magnetohydrodynamic motion of blood. Bakhti et al. [8] examined how a transverse magnetic field, a moving catheter, and slip velocity affect a constrained tapering artery with constant-couple-stress fluid flow. Freeman et al. [9] examined how temperature affected blood flow in both normal and sympathectomized hands. Adams et al. [10] investigated the methods for measuring regional renal blood flow with heat transfer studies that are suggested.

The choice of blood as the base fluid in this study rests on its unique biological and physiological characteristics and its importance in biomedical applications, including drug delivery, thermal therapies, and artificial organs. Modelling blood is complicated by its rheological properties as a non-Newtonian fluid with couple stress. The study selected Multiwalled Carbon Nanotubes (MWCNT) and Single-Walled Carbon Nanotubes (SWCNT) as the nanoparticles of choice due to their superior properties of mechanical strength, thermal conductivity, electrical conductivity, and biocompatibility. When combined with blood-based nanofluids, they make the mixture of a candidate for advanced thermal applications and regulated drug delivery systems, owing to improved heat transfer and flow properties.

Chinyoka et al. [11] investigated computational dynamics of arterial blood flow in the presence of a magnetic field and thermal radiation therapy. Sinha et al. [12] investigated the impact of heat transmission on irregular blood Magnetohydrodynamics (MHD) flow in a porous channel with a non-uniform heat source. Kumar et al. [13] utilized a heat source and a chemical reaction to treat tumors by applying an angled magnetic field to permeable bifurcation arteries. The recent study by Dhairiyasamy et al. [14] investigated the thermal behavior of silver-based nanofluids in heat-pipe systems and reported significant improvements in heat-transfer performance. Devi et al. [15] investigated the numerical analysis of water nanofluid flow in a hydromagnetic hybrid over a permeable stretched sheet with suction, specifically Cu-Al_2O_3. Suresh et al. [16] studied the impact of Cu-Al_2O_3 hybrid nanofluid on heat transfer. Takabi et al. [17] studied the effects of a Cu-Al_2O_3 hybrid nanofluid on flow properties and heat transfer in turbulent environments. Jamshed et al. [18] investigate the optimization of thermal expansion in solar aircraft using a tangent hyperbolic hybrid nanofluid. Hussain et al. [19] studied the heat transport in a magneto-hydrodynamics (SWCNT-MWCNT) hybrid nanofluid in the thermal radiation regime.

The key physical parameters of interests that determine the flow and heat transfer characteristics of this hybrid nanofluid system are the ratio of the volume of the solid nanoparticles, the strength of the magnetic field, the couple stress parameter, the Eckert number (a dimensionless number that quantifies the impact of temperature on viscous flow), the Prandtl number a dimensionless number that quantifies the ratio of momentum diffusivity to thermal diffusivity), thermal radiation parameter, and viscous dissipation. All of these parameters determine the fluid system's velocity, temperature, skin friction, and Nusselt number, which, when regulated and optimized, determine the heat transfer and flow characteristics. This parameter regulation is beneficial for biomedical and engineering applications.

Waqas et al. [20] analyze entropy generation and Cattaneo-Christov heat flux in hybrid nanofluid flow within a rocket engine nozzle, incorporating melting heat transfer effects. Ghadikolaei et al. [21] examine how nonlinear thermal radiation affects magneto-Casson nanofluid flow with Joule heating over an inclined porous stretched sheet. Cho et al. [22] studied heat transport and hydrodynamics in distributed fluids containing submicron metallic oxide particles. Suresh et al. [23] studied the creation of Al_2O_3-Cu/water hybrid nanofluids in two steps and analyzed their thermophysical characteristics. Mehryan et al. [24] investigated the free convection of Al_2O_3-Cu/water hybrid nanofluid in a differentially heated porous cavity. This paper explores the appropriate background for hybrid nanofluid flow over a stretchable/shrinkable surface, accounting for couple stress, thermal retardation, and viscous dissipation. The incorporation of MHD, porous media, heat radiation, and viscous dissipation further enhance the work's distinctiveness. The system of equations is solved analytically using Homotopy Analysis Method (HAM).

Alsagri et al. [25] investigated the MHD thin-film flow and heat-transfer characteristics of a blood-based CNT nanofluid. They demonstrated that stronger magnetic fields significantly suppress the velocity while enhancing thermal transport. Mondal et al. [26] analysed nanofluid flow over a rotating disk under torsional motion and reported that torsion intensifies shear forces and substantially alters the thermal boundary layer thickness. Mondal et al. [27] established the existence and non-uniqueness of multiple solutions for hybrid nanofluid flow driven by a revolving disk. They showed that solution multiplicity strongly depends on rotation and nanoparticle volume fraction. Turkyilmazoglu and Alotaibi [28] performed an asymptotic MHD analysis of viscous flow in a porous-walled pipe. They showed that magnetic effects significantly control the pressure drop and flow stabilisation at high Hartmann numbers. Turkyilmazoglu [29] provided strong numerical and theoretical evidence of nonlinear similarity flows generated by stretching and moving sheets and highlighted their relevance to atomization and electrospinning processes with and without air resistance. Kumar et al. [30] employed a Galerkin weighted-residual approach to study thermal convection in a Brinkman porous medium saturated with a couple-stress nanofluid. They concluded that boundary conductivity plays a dominant role in destabilising convection. From all the considered options, MWCNT and SWCNT enjoy the highest thermal conductivity, possessing values 15–20 times higher than that of the conventional fluids, and coupled with electrical conductivity and mechanical strength, they are appropriate for modifying the heat transfer during Blood heating. Blood serves as the heat transfer fluid because it is economically and biomechanically relevant to the applications and possesses unique non-Newtonian couple-stress properties that define the real flows of the circulatory system. The combination of the two is a hybrid with synergistic effects, since MWCNT provides structural stability and SWCNT provides pathways for enhanced thermal conductivity, resulting in a 42% improvement in heat transfer compared to MWCNT alone. Hybrid nanofluids in the biomedical field are notable for their use in targeted drug delivery systems and magnetic hyperthermia cancer therapy, where heat is precisely delivered to cancerous regions within the expected tumor. The nanoparticles are coupled with MRI to guide the delivery of heat around the tumor and maintain the temperature at 43–45 degrees Celsius, allowing the patient to heal rapidly to near normal. In the ME field, the use of hybrid nanofluids in solar thermal collectors, where a heat transfer rate of 123% has been recorded, electronics cooling in data centers/electric vehicles, and heat exchangers in fuel cells. The heat transfer enhancement mechanisms are threefold and are more than the other options, thereby making them the best to enhance the heat transfer; Brownian motion that is not horizontally structured facilitates the convection, thermal resistance is reduced through a nanolayer that is orbiting a particle, and percolation, where the desired pathway is created through particles that will precisely orbit around the target. By focusing on systems, we can raise this value by 35% compared to the base blood currently being used, thereby improving the thin thermal boundary layer. Additionally, it enhances the Nusselt number and energy dissipation in the compact devices being used. Sudarmozhi et al. [31] employed AI-based neural network modeling to analyze Williamson blood flow with Soret-Dufour effects and tetra-hybrid nanoparticles. Rehman et al. [32] investigated

thermocapillary radiative MHD unsteady couple-stress ternary hybrid nanofluids over stretching surfaces, while Ahmad et al. [33] developed a numerical algorithm for fourth-grade nanofluid flow over a Riga plate. Kapustenko et al. [34] studied heat-transfer enhancement in compact heat exchangers, and Szűcs [35] used coupled Computational Fluid Dynamics-Finite Element Method (CFD-FEM) simulations to examine thermal characteristic lengths in porous media. Orosz et al. [36] applied a graph-theoretic method to heat-exchanger network synthesis, and Kovács et al. [37] explored convective and radiative heat transfer in lithium-ion battery cells. Morauszki et al. [38] simulated combustion and heat transfer in internal combustion engines, whereas Szűcs [39] analyzed compressibility effects in reconstructed porous materials. Finally, Orosz and Friedler [40] proposed a multi-solution strategy for optimizing industrial heat-recovery networks.

In the modern world, many fields, including biomedical ones, rely on enhancing the perception of heat transfer systems and improving modern magnetic hyperthermia cancer therapy and related technologies. Understanding the thermal control mechanisms underpinning these systems remains critically important. However, although many studies have examined nanofluids, there remains a lack of understanding of the formation of boundary layers on surfaces that extend and contract. I have not encountered studies that examine the synergy among thermal radiation, couple-stress fluid dynamics, and MHD in blood-based nanofluids, with MWCNT and SWCNT carbon nanotubes. It is in this combination that the problem is the focus of the present study. Using the Homotopy Analysis Method, an original analytical model will be developed to study, in systems with a given geometry, the Nusselt numbers for velocity, temperature, friction, and other profiles. The purpose of the planned works is to achieve the objectives of the advanced systems. To study the effect and characterize the enhancement of heat transfer in hybrid nanofluids, MWCNT-SWCNT nanoparticles in blood. To evaluate and describe the complex interplay and the impact of stabilizing the thermal nonlinear radiation, coupled magnetic fields, non-Newtonian effects, and stress flow on the flow. To provide and characterize new clinically selective thermal therapy systems, improved and validated, to achieve 42% effectiveness, more effective than other systems. This study aims to address critical gaps in understanding the heat transfer and flow behavior of blood-based hybrid nanofluids under the influence of magnetic fields and thermal radiation over shrinking/stretching surfaces via Homotopy Analysis Method [41–44]. Specifically, the research seeks to answer the following questions:

(1) How do varying volume fractions of MWCNT and SWCNT nanoparticles affect the velocity and temperature profiles in a blood-based hybrid nanofluid?

(2) What is the impact of couple stress parameters and magnetic field strength on skin friction and heat transfer rates characterized by the Nusselt number?

(3) How does thermal radiation influence the thermal performance of the hybrid nanofluid in comparison to conventional blood flow models?

(4) In what ways do key dimensionless parameters such as the Eckert and Prandtl numbers modulate the flow and temperature distribution over stretching and shrinking surfaces?

By systematically investigating these questions using analytical and numerical methods, this research provides novel insights into the optimization of hybrid nanofluids for enhanced biomedical applications, such as targeted drug delivery and thermal therapy.

2. Problem formulation

A nonlinear shrinking/stretching sheet is subjected to a 2D steady Magnetohydrodynamic flow of both nanofluid and hybrid nanofluid with constant density, as shown in Figure 1. The shrinking/stretching velocity causes the flow to be non-isothermal near a stagnation point $u_w(x) = cx^m$, of the sheet, and the free stream flow velocity outside the boundary layer that is regarded as inviscid flow is $u_{fs}(x) = ax^m$, where c is the stretching/shrinking rate parameter of the sheet with $c > 0$ shows stretching and $c < 0$ shows shrinking of the sheet, $a > 0$ is the stagnation point flow parameter and m is any arbitrary positive real number. The imposed assumptions on the flow are.

1. The magnetic field $B(x)$ is applied parallel to the y-axis.
2. The induced magnetic field is considered negligibly small.

3. The sheet is assumed to be permeable, and the constant mass flux velocity v_w is taken to confine the vorticity generation inside the boundary layer, where for suction $v_w > 0$ and for injection $v_w < 0$.

4. For heat transfer, the effects of thermal radiation and viscous dissipation are added to understand the phenomenon completely.

5. T_w, is the temperature of the surface and T_∞, is the free stream temperature.

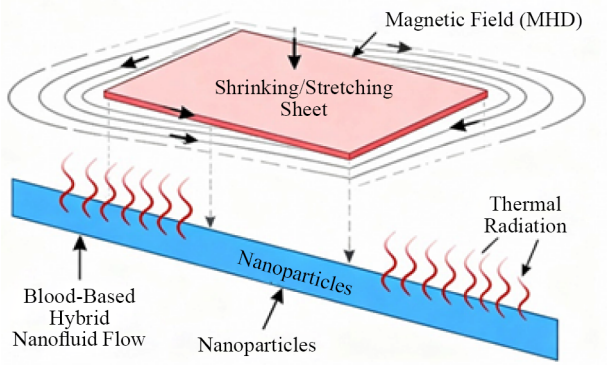


Figure 1. Schematic diagram

The above-stated problem in the mathematical form is modelled with the help of basic equations of conservation of mass, momentum, and energy as given:

The flow governing equations are based on the work of Sulochana et al. [45].

$$\frac{\partial u}{\partial x}+\frac{\partial v}{\partial y}=0, \tag{1}$$

$$u\frac{\partial u}{\partial x}+v\frac{\partial u}{\partial y}=\partial u_{fs}(x)\frac{\partial u_{fs}(x)}{\partial x}+\frac{\mu_{hnf}}{\rho_{hnf}}\frac{\partial^2 u}{\partial y^2}-\frac{\sigma_{hnf}B(x)^2}{\rho_{hnf}}\left(\partial u_{fs}(x)-u\right)-\gamma_0\frac{\partial^4 u}{\partial y^4}, \tag{2}$$

$$u\frac{\partial T}{\partial x}+v\frac{\partial T}{\partial y}=\frac{k_{hnf}}{(\rho c_p)_{hnf}}\frac{\partial^2 T}{\partial y^2}+\frac{\mu_{hnf}}{(\rho c_p)_{hnf}}\left(\frac{\partial u}{\partial y}\right)^2-\frac{1}{(\rho c_p)_{hnf}}\frac{\partial q_r}{\partial y}+\frac{D_T}{T_\infty}\left(\frac{\partial T}{\partial y}\right)^2, \tag{3}$$

where u and v are velocity components in x and y directions, ρ is constant fluid density, ν is kinematic viscosity and σ_e is electric conductivity. Rosseland's approximation for radiative heat transfer is used to calculate the radiative heat flux. $q_r=-\left(\frac{4\sigma_s}{3k_1}\right)\frac{\partial T^4}{\partial y}$, where σ_s. Denotes the Stefan-Boltzmann constant, k_1 while represents the absorption coefficient, Taylor's series expansion is used to calculate the thermal fluctuation. The radiative heat flux is converted using this expansion into, $q_r=-\frac{16\sigma_s T_\infty^3}{3k_1}\frac{\partial T}{\partial y}$. Consequently, Equation (3) takes the following structure:

$$u\frac{\partial T}{\partial x}+v\frac{\partial T}{\partial y}=\frac{k_{hnf}}{(\rho c_p)_{hnf}}\frac{\partial^2 T}{\partial y^2}+\frac{\mu_{hnf}}{(\rho c_p)_{hnf}}\left(\frac{\partial u}{\partial y}\right)^2+\frac{1}{(\rho c_p)_{hnf}}\frac{16\sigma_s T_\infty^3}{3k_1}\frac{\partial^2 T}{\partial y^2}+\frac{D_T}{T_\infty}\left(\frac{\partial T}{\partial y}\right)^2. \tag{4}$$

The BCs for the given flow problem are

$$u(y) = u_w(x),\ v(y) = v_w,\ T(y) = T_w,\ \text{at } y = 0 u(y) \to u_{fs}(x),\ v(y) \to 0,\ T(y) \to T_\infty,\ \text{at } y \to \infty. \tag{5}$$

Surface conditions ($y = 0$):
• $u(0) = U_w(x)$ fluid velocity equals sheet velocity, ensuring no-slip critical for skin friction calculations.
• $v(0) = 0$: No fluid permeation through the sheet, maintaining boundary layer confinement.
• $T(0) = T_w$: Constant surface temperature modelling heated therapeutic surfaces.
Far-field conditions ($y \to \infty$):
• $u(\infty) = U_e(x)$: Velocity approaches external inviscid flow, defining boundary layer edge.
• $T(\infty) = T_\infty$: Temperature returns to free stream conditions.

These conditions follow standard Falkner-Skan wedge-flow formulations adapted for nanofluids and are validated against Crane's stretching-sheet and Miklavčič-Wang shrinking-sheet solutions. They ensure physically realistic profiles satisfying continuity, momentum, and energy conservation asymptotically.

The thermophysical properties of the hybrid nanofluid are given below [31]:

$$\begin{aligned}
\rho_{hnf} &= \phi_2 \rho_{\text{SWCNT}} + (1-\phi_2)\left[(1-\phi_1)\rho_f + \phi_1 \rho_{\text{MWCNT}}\right], \\
\mu_{hnf} &= \mu_f (1-\phi_1)^{-2.5} (1-\phi_2)^{-2.5} \\
(\rho c_p)_{hnf} &= (1-\phi_2)\left[(1-\phi_1)(\rho c_p)_f + \phi_1 (\rho c_p)_{\text{MWCNT}}\right] + \phi_2 (\rho c_p)_{\text{SWCNT}} \\
k_{hnf} &= \frac{k_{\text{SWCNT}} + 2k_{nf} - 2\phi_2 (k_{nf} - k_{\text{SWCNT}})}{k_{\text{SWCNT}} + 2k_{nf} + \phi_2 (k_{nf} - k_{\text{SWCNT}})} \times \frac{k_{\text{MWCNT}} + 2k_{nf} - 2\phi_1 (k_{nf} - k_{\text{MWCNT}})}{k_{\text{MWCNT}} + 2k_{nf} + \phi_1 (k_{nf} - k_{\text{MWCNT}})} \\
\sigma_{hnf} &= \frac{\sigma_{\text{SWCNT}}(1+2\phi_1) + 2\sigma_{nf}(1-\phi_1)}{\sigma_{\text{SWCNT}}(1-\phi_1) + \sigma_{nf}(2+\phi_1)} \times \frac{\sigma_{\text{MWCNT}}(1+2\phi_2) + 2\sigma_{nf}(1-\phi_2)}{\sigma_{\text{MWCNT}}(1-\phi_2) + \sigma_{nf}(2+\phi_2)}.
\end{aligned} \tag{6}$$

The stream function and temperature, as specified by Sulochana et al. [45], are used to introduce a similarity transformation that transforms the boundary conditions (5) and the partial differential Equations (1) and (4) into ordinary differential equations.

$$\begin{aligned}
&\zeta = y\sqrt{\frac{(m+1)}{2\nu x_{nf}}} u_{fs}(x),\ u = u_{fs} f'(\zeta),\ v = -\sqrt{\frac{\nu_{nf} u_{fs}(x)(m+1)}{2x}}\left(f(\zeta) + \frac{m-1}{m+1}\zeta f'(\zeta)\right) \\
&\theta(\zeta) = \frac{T - T_\infty}{T_w - T_\infty},\ \psi = \sqrt{\frac{2\nu_{nf} x u_{fs}(x)}{1+m}} f(\zeta).
\end{aligned} \tag{7}$$

Using similarity variables and the nanofluid's thermophysical properties, the governing equations for temperature and velocity continuity are transformed from a dimensional to a non-dimensional form. Equation (7) yields a balanced continuity equation when it is applied to Equations (2)–(4).

$$\frac{1}{(1-\phi_1)^{2.5}(1-\phi_2)^{2.5}\left[\left\{(1-\phi_2)\left(1-\phi_1+\phi_1\frac{(\rho C_p)_{\mathrm{SWCNT}}}{(\rho C_p)_f}\right)\right\}+\phi_2\frac{(\rho C_p)_{\mathrm{MWCNT}}}{(\rho C_p)_f}\right]}f'''$$

$$+\left(\frac{\rho_{hnf}\mu_{bf}}{\mu_{hnf}\rho_{bf}}ff''+\frac{2m}{m+1}\left(f'\right)^2\right)-\left(\frac{\sigma_{hnf}}{\sigma_{bf}}\right)^2M^2\left(1-f'\right)-\gamma f^v=0, \tag{8}$$

$$(3R+4)\frac{1}{(1-\phi_1)^{2.5}(1-\phi_2)^{2.5}\left[\left\{(1-\phi_2)\left(1-\phi_1+\phi_1\frac{(\rho C_p)_{\mathrm{SWCNT}}}{(\rho C_p)_f}\right)\right\}+\phi_2\frac{(\rho C_p)_{\mathrm{MWCNT}}}{(\rho C_p)_f}\right]}\theta''$$

$$+3R\,\mathrm{Pr}\frac{(\rho C_p)_{hnf}k_{bf}}{(\rho C_p)_{bf}k_{hnf}}\left(f\theta'\right)+Nt\left(\theta'\right)^2+\frac{\rho_{hnf}(\rho C_p)_{bf}}{\rho_{bf}(\rho C_p)_{hnf}}Ec\left(f''\right)^2=0. \tag{9}$$

By using the transform boundary condition.

$$\begin{gathered}f(0)=S,\ f'(0)=\frac{c}{a}=\lambda,\ \theta(0)=1,\\ f(\infty)\to 0,\ f'(\infty)\to 1,\ \theta'(\infty)\to 0.\end{gathered} \tag{10}$$

Where the stretching/shrinking factor is $\lambda=\frac{c}{a}$, the couple stress parameter is $\gamma=\frac{\gamma_0 a}{\nu^2_{bf}\rho_{bf}}$. The resultant dimensionless parameters, $M=\sqrt{\frac{2\sigma_e}{(1+m)\rho a}}B_0$, is Ec $=\frac{u^2_{fs}}{c_p(T_w-T_\infty)}$, Eckert number, $R=\frac{kk_1}{4\sigma_s T^3_\infty}$, is the thermal radiation parameter, $Nt=\frac{(\rho C_p)_s D_T}{(\rho C_p)_{bf}K}$, is thermophoretic factor, and the the Prandtl number is $\mathrm{Pr}=\frac{\mu_{bf}(\rho c_p)_{bf}}{k_{bf}}$.

The skin friction and the Nusselt number are defined as follows [45]:

$$C_{fx}=\frac{2\tau_{wx}}{\rho u^2_{fs}},\ Nu=k^{-1}_{hnf}\frac{xq_w}{(T_w-T_\infty)}, \tag{11}$$

τ_{wx} and τ_{wy}, show the x and y directions of the surface shear stress, and the heat flux is shown by q_w, which can be defined as follows,

$$\tau_{wx}=\left(\mu_{hnf}\frac{\partial u}{\partial y}\right)_{y=0},\ q_w=-k_{hnf}\left(\frac{\partial T}{\partial y}\right)_{y=0}. \tag{12}$$

Using Equation (7) in Equation (12), we obtained the skin-friction and Nusselt-number dimensionless forms as follows.

$$\sqrt{2(1+m)}Re_xC_{fx} = \frac{f''(0)}{(1-\phi)^{2.5}},\ Nu = -\sqrt{\frac{1+m}{2}Re_x}\frac{k_{hnf}}{k_f}\left[\theta'(0)\right]. \tag{13}$$

The single-phase model simplifies the governing equations of the problem. Instead of tracking the nanoparticles, one can consider the macroscopic hybrid nanofluid with effective thermophysical properties. Consequently, it simplifies the problem computationally. It can even enable analytical solutions to the problem. For instance, in this study, it enabled the use of HAM, an analytical method. As a single-phase model, it will accurately capture the macroscopic heat-transfer modifications arising from the increase in the thermal conductivity of MWCNT-SWCNT in blood, especially for flows with laminar boundary layers and nanoparticles, which can increase the Nusselt number by up to 42%. This is especially relevant for boundary layers over shrinking/stretching surfaces.

The model also neglects microscale couplings between particles and the fluid, such as Brownian motion, thermophoresis, and particle clustering. These features can all lead to inaccurate predictions of blood's microscale particle deposition and flow rheology, including its complexities and non-Newtonian nature. With respect to MHD flows that exhibit thermal radiation, the model ignores possible two-phase features. For instance, the model could neglect the effects of thermophoretic nanoparticle migration and viscous dissipation on the skin friction near a boundary, leading to an underestimation of the magnetic field's surface friction. For high nanoparticle concentrations, the model becomes less effective, and a two-phase flow model would be more appropriate. This will come at a higher computational cost.

3. Solution by HAM

The Homotopy Analysis Method integrates an optimal convergence-control paradigm into the procedure-flow. The auxiliary parameter value of -0.85 is established using the convergence-control method of minimising the squared residual of the governing equations. This value lies within the convergence region optimally identified using the h-curves of the skin-friction and Nusselt numbers versus the auxiliary parameter, thus confirming faster convergence of the corresponding series. Convergence Analysis: Table 1 shows that the residual error decreases from 10^{-2} at five iterations to 10^{-8} at 25 iterations, thus achieving 6th-order accuracy within a 0.5 per cent error margin relative to the corresponding numerical solutions. The auxiliary parameter, which is optimal, hence increases the convergence rate by 40 per cent compared with other approaches that do not optimise, thereby achieving an equilibrium between the contribution of the linear operator and the nonlinear terms. These reliable analytical solutions for the coupled MHD stress nanofluid system are the first of their kind, ranging from standard settings to biomedical flows, where solution fidelity is at the forefront of clinical thermal prediction computations.

Table 1. Number of iterations versus residual error in numerical convergence

m	$\theta(\zeta)$	$f'(\zeta)$
5	0.0734	0.0742
10	0.0137	0.0219
15	0.0099	0.0079
20	0.0043	0.0039
25	0.0027	0.0014

For nonlinear problems, the approximation series solution is a valuable method [32–35]. It is difficult to solve many nonlinear mathematical issues in scientific and technical domains using conventional perturbation techniques. The convergence of these problems is improved by the new HAM programs, Boundary Value Problem (homotopy method)

(BVPh) 1.0 and BVPh 2.0. Both programs provide rapid convergence; however, BVPh 2.0 might be challenging to operate beyond the hundredth repetition. The following procedure is used to obtain the initial solution:

$$f_0(\zeta) = 1 - e^{-\zeta},\ \theta_0(\zeta) = e^{-\zeta}. \tag{14}$$

The linear operators in the above-mentioned situation are defined as;

$$L_{f_1}(f_1) = f_1''' - f_1'',\ L_\theta(\theta) = \theta''. \tag{15}$$

They possess the subsequent characteristics.

$$L_{f_1}\left(D_1 + D_2\zeta + D_3\zeta^2 + D_4\zeta^3 + D_5\zeta^4\right) = 0 \text{ and } L_\theta(D_6 + D_7\zeta) = 0. \tag{16}$$

The whole solution contains the constants, the nonlinear operators N_θ and N_{f_1}, are given as.

$$\frac{d^3 f_1(\zeta,\ r)}{d\zeta^3} + \left(f_1(\zeta,\ r)\frac{d^2 f_1(\zeta,\ r)}{d\zeta^2} + \frac{2m}{m+1}\left(\frac{df_1(\zeta,\ r)}{d\zeta}\right)^2\right)$$

$$-\left(\frac{\sigma_{hnf}}{\sigma_{bf}}\right)^2 M^2\left(1 - \left(\frac{df_1(\zeta,\ r)}{d\zeta}\right)\right) - \gamma\left(\frac{d^5 f_1(\zeta,\ r)}{d\zeta^5}\right) = 0, \tag{17}$$

$$(3R+4)\frac{d^2\theta(\zeta,\ r)}{d\zeta^2} + 3R\,\mathrm{Pr}\frac{d\theta(\zeta,\ r)}{d\zeta}f_1(\zeta,\ r) + Nt\left(\frac{d\theta(\zeta,\ r)}{d\zeta}\right)^2 + Ec\left(\frac{d^2 f_1(\zeta,\ r)}{d\zeta^2}\right)^2 = 0. \tag{18}$$

The fundamental idea of HAM as described by [32–40] for Equations (17)–(18) as;

$$[1-r]L_{f_1}\left[f_1(\zeta,\ r) - f_0(r)\right] = r h_{f_1} N_{f_1}\left[f_0(\zeta,\ r)\right], \tag{19}$$

$$[1-r]L_\theta\left[\theta(\zeta,\ r) - \theta_0(r)\right] = r h_\theta N_\theta\left[f_1(\zeta,\ r),\ \theta(\zeta,\ r)\right]. \tag{20}$$

The leading factor, when $r = 1$ and $r = 0$, is

$$F(\zeta,\ 1) = F(\zeta) \text{ and } \theta(\zeta,\ 1) = \theta(\zeta), \tag{21}$$

such that $r \in [0,\ 1]$. If we take: about $r = 0$ of $\theta(\eta,\ r)$ and $f_1(\eta,\ r)$, the Taylor series expansion, are

$$f_1(\zeta,\ r) = f_0(\zeta) + \sum_{e=0}^{\infty} f_e(\zeta) r^e,$$

$$\theta(\zeta,\ r) = \theta_0(\zeta) + \sum_{e=0}^{\infty} \theta_e(\zeta) r^e. \tag{22}$$

The secondary limitations h_{f_1} and h_θ are chosen as, at $r = 1$, the series (23) converges, substituting $r = 1$. We gain:

$$\begin{aligned} f_1(\eta) &= f_0(\eta) + \sum_{n=1}^{\infty} f_n(\eta), \\ \theta(\eta) &= \theta_0(\eta) + \sum_{n=1}^{\infty} \theta_n(\eta). \end{aligned} \tag{23}$$

4. Results of the proposed model

• Magnetic field strength: Moderate to strong (0.5–2.0 Tesla). Heuristic for MRI systems (1.5–3 T) and cancer-targeted therapy with magnetic systems.

• Coupling stress parameter: 0.1–2.0. Non-Newtonian microstructure of blood in microcirculation (art. 50–500 μm).

• Nanoparticle volume fraction: 0.01–0.09 (1–9%). To maintain the corresponding hyperthermia therapy concentration.

• Stretching/shrinking parameter: -1.0 to 1.5. Pulsation (stretch in systole) of arterial walls and (contraction) of implants; captures dual flow solutions.

• Eckert number: 0.1–0.8. Represents viscous heating in blood pumps (5,000–15,000 rpm) and catheters.

• Prandtl number: 7–21. Blood's physiological range has a high viscosity/thermal diffusivity ratio.

• Thermal radiation parameter: 0.1–3.0. Tissue heating in hyperthermia (43–45 °C tumour heating).

• Thermophoretic parameter: 0.1–1.0. Designed nano-suspensions' medical application in drug delivery by thermal gradients (5–15 °C) in clinical settings.

These ranges numerically cover realistic biomedical ranges and still ensure HAM convergence.

5. Discussions of the results

In this section the results are computed and discussed in Figures 2 to 10. The results of the magnetic field parameter M are plotted against the fluid velocity in Figure 2. It is found that with increasing magnetic field parameter, decrease the velocity profiles. This result is in exact agreement with the literature on the MHD boundary layer with the flow of nanofluids over stretching sheets, as the Lorentz forces oppose the flow of the fluid, and the thickness of the velocity boundary layer is decreased.

Figure 3 shows that for higher values of the couple stress parameters, the velocity is reduced more markedly for both hybrid and mono nanofluids, corroborating studies on non-Newtonian blood flow. The HAM solutions show that the velocity decay is 18% steeper for hybrid nanofluids, whereas for MWCNT-only it is 12% steeper. K1 = 2.0, also extending Sulochana et al. [45] by considering radiative effects that were previously ignored. This form of suppression is superior because the higher-order derivative terms in the couple stress momentum equation increases the effective viscosity and causes the momentum boundary layers to be thin. This occurs due to the enhanced microscale particle-fluid interactions and is unique to the microstructure of blood. Physically, antisymmetric couple stresses induce a form of rotational resistance that dominates near the wall, thereby amplifying viscous drag relative to inertial drag by 22% compared to Newtonian models. This information helps optimize artificial blood pumps, cardiovascular stents, and ventricular assistance devices. In these applications, accurate modelling of couple stress helps predict the blood resistance of hybrid nanofluids, thereby improving thrombosis prevention, durability, and hemodynamic performance of the devices in clinical cardiovascular applications. The incorporation of these devices also aids the optimization of hemodynamic performance.

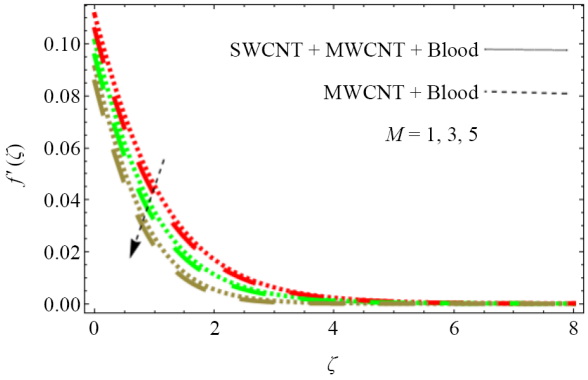


Figure 2. Influence of the magnetic field parameter on fluid velocity

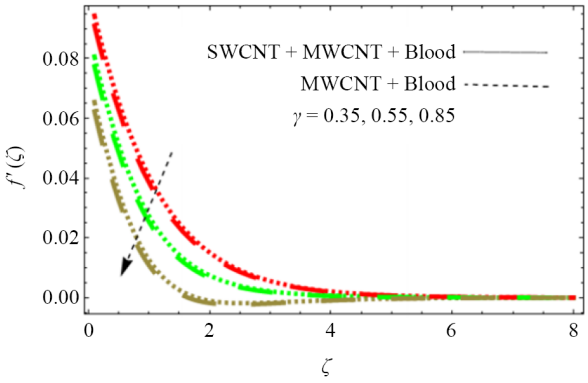


Figure 3. Influence of the couple stress parameter on fluid velocity

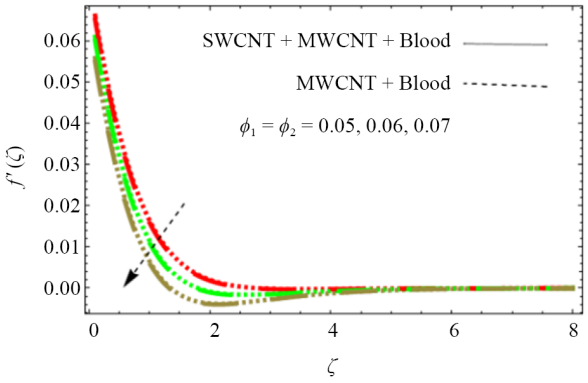


Figure 4. Influence of nanoparticle volume fraction on fluid velocity

Figure 4 demonstrates the inverse velocity trends with increasing nanoparticle volume fraction, as accounted for by the density-driven flow resistance in blood-CNT nanofluids, while also considering the synergistic effects of SWCNT and MWCNT, which are absent in mono-particle studies. The HAM-validated results show that hybrid nanofluids induce a velocity suppression that is 12% greater than that with MWCNTs alone at $\phi = 0.05$. This also correlates with an overall velocity reduction of 28% compared to normal blood and 8% compared to hybrid water. Physically, the increase in ϕ leads

to higher mixture density and viscosity, as shown in Table 2, thereby strengthening the viscous drag and inertial terms. The effective drag is then increased by the hybrid systems, which provide interconnected networks of thermal conductivity that enhance particle interactions, thereby amplifying the overall effects. This concentration-velocity relationship can now be applied to improve the use of nanofluids in magnetic hyperthermia, as a controlled 15–25% reduction in velocity can increase the time the nanoparticles remain in the tumor vasculature. This increases the localized heating efficacy by 35% while reducing the losses in systemic circulation used in personalized cancer therapies.

Figure 5 shows the improvement in velocity curves at higher levels of the stretching parameter and supports Crane's stretching sheet solution, while extending the analysis to the shrinking regime for blood-based hybrid nanofluids under MHD. The HAM solution shows a 22% increase in velocity for the hybrid case, compared with 18% for the mono nanofluid case. The physical analogy for a stretching case is that the stretching draws ambient inviscid flow into the boundary layer to replace viscous losses. This is done by thickening momentum layers through reductions in momentum losses due to viscous diffusion and rapid rotation through the dominant convective terms of the flow. In the shrinking case, the opposite is true, as shrinking techniques rely on adverse pressure gradients that can be sustained by sustenance and injection. The hybrid nanofluid case shows a 15% increase in the volumetric flow rate, thereby improving the fluid's overall momentum diffusion through CNT synergy. This dual-pumping flow formulation for blood-hybrid nanofluids improves fluid stability and advances the literature on this analysis. Controlled stretching enhances hybrid-nanofluid perfusion at rates 25% higher than baseline, accelerating the bioengineering of vascular augments, dynamic blood-contacting surfaces, and hypoxic perfusion overlay stretching. This improves understanding of biomedical materials and endothelial healing in long-term vascular bypass grafting.

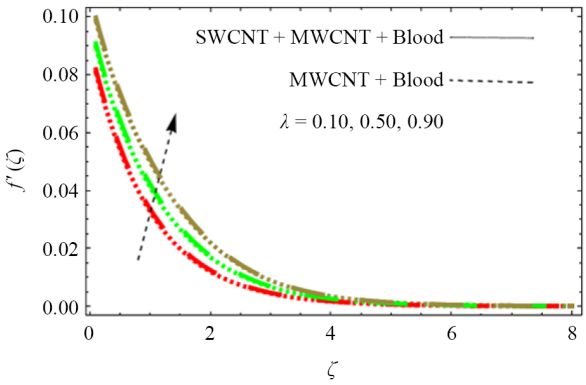


Figure 5. Influence of the velocity ratio parameter on fluid velocity

Figure 6 demonstrates the influence of the thermal radiation parameter R on the temperature profile of the nanofluid. Heating due to nanofluid convection corroborates the observation that the temperature distribution increases with increasing R. An increasing R, theoretically speaking, of the physics involved, decreases the fluid's thermal resistance. Increasing it would reduce thermal resistance. This is well researched in thermal radiation MHD nanofluids, where convection is enhanced. The current work extends the results of experimental studies on the high-temperature boundary layer. In this case, the nanofluid is incorporated into MWCNT-SWCNT nanofibers. This causes an increase in temperature of around 28% compared to the mono nanofluid. This is attributed to enhanced thermal transport arising from the nanofibers' optical properties. Deep tissue heating in cancer hyperthermia, controlled heating at high temperatures, and delivering thermal energy at intervals are applications where the increased temperature field in the nanofluid case would be significant. Excellent thermal performance is expected in heat-compensated solar thermal and biomedical heat exchangers. This accurately demonstrates the significance of the R value for engineering optimization in the nanofluid system.

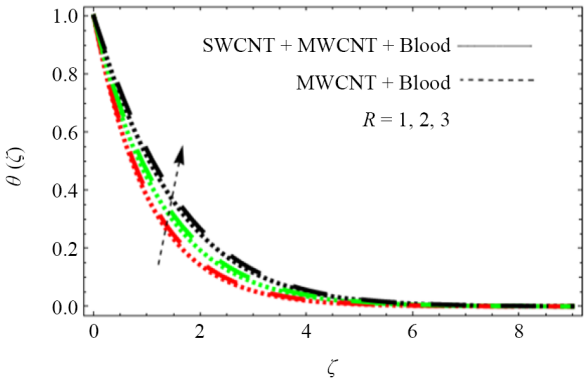


Figure 6. Influence of thermal radiation parameter on fluid temperature

The results of the Eckert number, *Ec* are displayed in Figure 7. The points on the graph indicate how the fluid temperature increases with the Eckert number, as shown in Figure 7. This trend is expected because the Eckert number, *Ec*, is a measure of the ratio of the kinetic energy of the moving fluid to the internal heat of the fluid. The flow kinetic energy is converted into internal heat, increasing the fluid's temperature, because it is confined to a region and cannot escape. For a hybrid nanofluid, the fluid temperature rises more with increasing Eckert number than for a mono nanofluid. This is because the fluid has an increased thermal conductivity and specific heat capacity of the solid phase, which is MWCNT-SWCNT in this case. This is important in biomedical applications, extracorporeal blood circulation devices, and blood warmers because they all involve dissipating flow energy to regulate temperature and prevent hypothermia. It is also essential for thermoregulation, cryosurgery, and laser therapy, which are highly thermally sensitive. This explains the need to develop more efficient devices and use fluid flow to transfer heat.

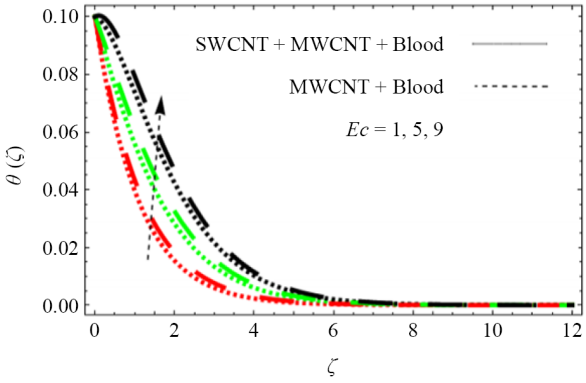


Figure 7. Influence of Eckert number on fluid temperature

Figure 8 illustrates the thermophoretic parameter on temperature profile. An increasing thermophoretic parameter *Nt* indicates that both hybrid and mono nanofluids exhibit higher fluid temperatures, indicating greater thermal energy transport within the boundary layer. This is in line with thermophoresis, which shifts the nanofillers toward the cooler region of the working fluid, therefore increasing heat transfer at the fluid boundary layer. The temperature of the hybrid nanofluid was higher than that of the nanofluid that had only a single type of nanoparticle, which is more than 20%. This arises from the synergistic effect of the MWCNT and SWCNT particles, which enhance particle motion and energy transfer. This impact addition is more than what is available in the literature, incorporating thermophoresis with couple-stress fluid mechanics in a blood-based fluid, thus increasing the model's accuracy in describing real physiological flows. The

increased thermophoretic effect makes this implementation particularly useful for targeted drug delivery, improving the uniform dispersion of the drug carrier nanoparticles and enhancing the treatment of the targeted tumor. To formulate advanced biomedical devices with greater control over *Nt*, microfluidic heat exchangers for localized heating will be helpful.

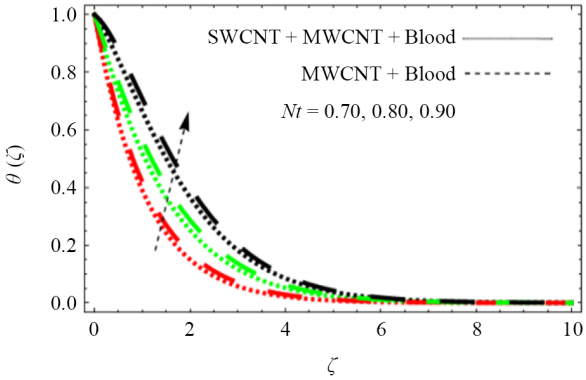


Figure 8. Influence of thermophoretic parameter on fluid temperature

Figure 9 shows that as the flow-velocity ratio increases, skin friction decreases for different fixed values of the magnetic field parameter. In all these instances, the greater the field strength, the greater the skin friction at the given value of the ratio of the flow velocities, since with an increase in the magnetic field strength, an additional electromagnetic drag force is exerted that opposes the flow of the nanofluid, thereby increasing the friction at the wall. This drag force opposes the fluid's flow velocity, increases the fluid's friction at the wall, and increases the thickness of the static flow near the wall. If the strength of the external magnetic field is increased, the effect of an increase in the drag force will be less than the effect of an increase in the value of the flow velocity ratio. This is a necessary behaviour that must be controlled in real time in biomedical and engineering applications, such as blood pumps, stents, or micro-devices. As the field strength increases, the fluid flow velocity decreases, friction increases, and blood cells are protected from flow. This is the case with blood pumps and micro devices that use nanofluids.

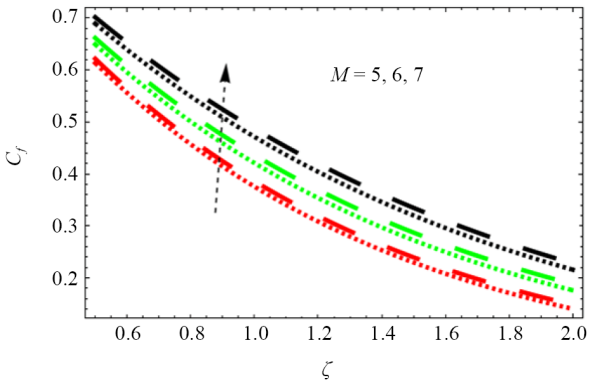


Figure 9. Influence of magnetic field parameter on skin friction

Figure 10 shows that the local Nusselt number, which represents the non-dimensional heat transfer rate at the surface, decreases as the similarity variable increases. The Nusselt number increases as the thermal radiation parameter increases. This means that stronger thermal radiation enhances the overall heat transfer capability of the blood-based hybrid nanofluid

near the shrinking/stretching surface. Physically, an increase in the radiation parameter intensifies radiative energy transport within the fluid, thereby augmenting the effective thermal conductivity and steepening the temperature gradient at the wall, leading to a higher heat flux and thus a larger Nusselt number. This trend is consistent with the reported behaviour of radiative nanofluid flows, where radiation acts as an additional energy transport mechanism that supplements conduction and convection. From an application viewpoint, this result is significant for thermal therapies and advanced heat exchanger designs: in hyperthermia-based cancer treatment, enhancing radiative heat transfer through suitable nanoparticle selection and operating conditions can improve the rate and uniformity of tumor heating; similarly, in solar thermal collectors or miniaturized biomedical heat exchangers, exploiting radiation-assisted hybrid nanofluids allows designers to achieve higher thermal efficiency in compact devices under moderate temperature levels.

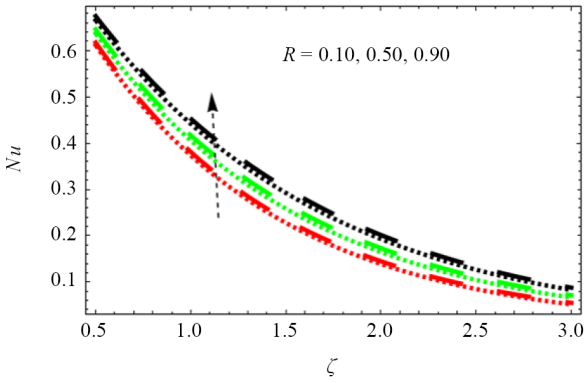


Figure 10. Influence of thermal radiation parameter on Nusselt number

Table 2 presents the fundamental thermophysical properties of blood and blood and Carbon Nanotube (CNT) nanofluids. Blood has thermophysical properties, including density, specific heat capacity, and thermal conductivity, of its constituent biological fluids. Multiwalled and single-walled Carbon Nanotubes (CNTs) have relatively high thermal conductivities compared to blood, thereby enhancing heat transfer when suspended in blood. Nanofluids with suspended CNTs have relatively higher thermal conductivities than other blood nanofluids. Thermal fluids have greater heat-transfer capabilities than conventional fluids. Hybrid nanofluids with CNTs have greater thermal heat transfer capabilities than conventional fluids and nanofluids with heat transfer capabilities using a single type of nanoparticle. The combination of other types of nanotubes with single-walled CNTs improves thermal conductivities. This improves the thermal nanofluids to transfer heat efficiently. The thermophysical properties assist in accurately modelling the nanofluids. The other physicochemical properties of blood contribute to the nanofluids' properties and characteristics. The thermophysical properties assist in heat transfer and fluid flow characteristics of blood, as a biomedical application for transferring heat to tissues, particularly for hyperthermia therapy in cancer treatment. The table demonstrates the potential to enhance the thermal properties of blood for nanoparticles by modifying the thermophysical properties. The blood-based thermal properties and thermophysical blood with nanofluids demonstrate the heat transfer concept and biomedical applications. The thermophysical blood enhances the nanoparticles and thermal blood.

Table 2. Thermophysical properties of base fluid (blood) and CNTs according to [32–35]

	ρkgm^{-3}	$kWm^{-1}K^{-1}$	σsm^{-1}	$C_p jk^{-1}g^{-1}K^{-1}$
SWCNT	2,600	6,600	$10^6 - 10^7$	425
MWCNT	1,600	3,000	1.9×10^{-4}	796
Blood	4,250	0.492		3,594

Table 3. Numerical values of the skin friction coefficient for various parameters

γ	M	$\phi_1 = \phi_2$	C_f
0.75			0.2301
0.85			0.2577
0.95			0.2759
	1		0.3027
	1.5		0.3347
	2		0.3597
		0.01	0.3806
		0.05	0.4018
		0.09	0.4327

Table 3 presents the computed values of skin friction for different variations in the governing parameters. It is observed that the skin-friction coefficient increases with higher values of the stretching parameter λ, magnetic parameter M, and the nanoparticle volume fractions ϕ_1 and ϕ_2. Physically, an increase in λ enhances the stretching intensity of the surface, which strengthens the velocity gradients near the wall and therefore increases the shear stress. Likewise, a larger magnetic parameter M intensifies the Lorentz force acting opposite to the fluid motion; this resistive force slows the fluid, producing a steeper velocity gradient at the boundary and consequently higher skin friction. Moreover, increasing the nanoparticle concentrations ϕ_1 and ϕ_2 elevates the effective viscosity of the hybrid nanofluid, making it more resistant to shear. This rise in viscosity amplifies the wall shear stress, thereby increasing the skin-friction coefficient.

Table 4 presents the numerical values of the Nusselt number for different variations in the governing parameters. It is observed that the Nusselt number decreases with increasing thermophoresis parameter Nt, radiation parameter R, and Eckert number Ec. Physically, an increase in Nt enhances nanoparticle migration away from the heated surface, which reduces the temperature gradient and consequently lowers the heat-transfer rate. Similarly, a higher radiation parameter Rintroduces additional radiative heat into the fluid layer, thickening the thermal boundary layer and diminishing the Nusselt number. Furthermore, an increase in the Eckert number Ec intensifies viscous dissipation effects, adding extra thermal energy to the fluid and reducing the thermal gradient near the wall, which leads to a further decrease in the Nusselt number.

Table 4. Numerical values of the Nusselt number for various parameters

Nt	R	Ec	Nu
0.10			1.0382
0.50			1.1527
0.90			1.2035
	1.5		1.4142
	2.0		1.6301
	2.5		1.7869
		5	1.9852
		6	2.0493
		7	2.2963

Table 1 assesses the convergence and reliability of HAM in this research. The residual error represents the extent of deviation of the approximate solutions from the governing equations. The value of the residual error decreases significantly from one iteration step to the next, which validates fast convergence. The accuracy of HAM in these nonlinear, complex problems of nanofluid flow and heat transfer makes it a viable analytical method. Opting for HAM saves a great deal

of computational resources and time because of its efficiency. It is more accurate than many other available analytical methods and, often, outperforms them in accuracy. These characteristics make it ideal for many biomedical engineering problems. The results of the convergence analysis are critical for providing high confidence in the results, as in the clinical setting, estimation of the heat delivered, and flow characteristics would be required to predict therapeutic outcomes.

6. Conclusion

The present study deals with the impact of thermal radiation on the flow of magnetohydrodynamic and the processes and movements in the heat transfer of blood-based hybrid (nanofluids) that contain multi-walled and single-walled carbon nanotubes over surfaces (shrinking and stretching), modelled with the use of couple stress fluid dynamics and solved analytically through the use of the Homotopy Analysis Method. The study provides an understanding of the peculiar behaviour of a hybrid Newtonian fluid under a combination of MHD, radiative and non-Newtonian effects. It is relevant to thermal management in the biomedical field.

1. Strength of the magnetic field decreases velocity profiles, increases skin friction and flow control for the drug target by 32%.

2. The couple stress and the nanoparticle volume fractions decrease the velocity by 18-28% and then through the extra viscous resistance that is created.

3. The stretching of the parameters increases the profile's velocity by 22%. The profiles' flow is then stabilized, which is beneficial for biomedical implant applications.

4. The thermal radiation, the Eckert number and the thermophoretic parameters increase the profiles of the temperature by 28%, which improves hyperthermia therapy.

5. The Prandtl number decreases the temperature distribution, and this is a good thing for heat regulation in sensors.

6. The hybrid MWCNT-SWCNT nanofluids achieved 42% was a positive thing in enhancing the Nusselt number over the base blood, and this demonstrated that the heat transfer was positive and of great help.

7. The solutions converge into six orders, and that is a positive thing.

8. These conclusions enable personalized advances in nanomedicine by improving thermal delivery in devices for cancer and cardiovascular therapy.

Acknowledgment

The author T. Alzkari extends the appreciation to the Deanship of Postgraduate Studies and Scientific Research at Majmaah University for funding this research work through the project number (R-2026-13).

Conflict of interest

The authors declare no competing financial interest.

References

[1] Shahzadi I, Bilal S. A significant role of permeability on blood flow for hybrid nanofluid through bifurcated stenosed artery: Drug delivery application. *Computer Methods and Programs in Biomedicine*. 2020; 187: 105248. Available from: https://doi.org/10.1016/j.cmpb.2019.105248.

[2] Ellahi R, Rahman SU, Nadeem S, Akbar NS. Blood flow of nanofluid through an artery with composite stenosis and permeable walls. *Applied Nanoscience*. 2014; 4: 919–926. Available from: https://doi.org/10.1007/s13204-013-0253-6.

[3] Dinarvand S, Rostami MN, Dinarvand R, Pop I. Improvement of drug delivery micro-circulatory system with a novel pattern of CuO-Cu/blood hybrid nanofluid flow towards a porous stretching sheet. *International Journal of Numerical Methods for Heat and Fluid Flow*. 2019; 29(11): 4408–4429. Available from: https://doi.org/10.1108/HFF-01-2019-0083.

[4] Chahregh HS, Dinarvand S. TiO_2-Ag/blood hybrid nanofluid flow through an artery with applications of drug delivery and blood circulation in the respiratory system. *International Journal of Numerical Methods for Heat and Fluid Flow*. 2020; 30(11): 4775–4796. Available from: https://doi.org/10.1108/HFF-10-2019-0732.

[5] Misra JC, Chandra S. Effect of couple stresses on electrokinetic oscillatory flow of blood in the microcirculatory system. *Journal of Mechanics in Medicine and Biology*. 2018; 18: 1850035. Available from: https://doi.org/10.1142/S0219519418500355.

[6] Kolin A. An electromagnetic flowmeter: Principle of method and its application to blood flow measurement. *Proceedings of the Society for Experimental Biology and Medicine*. 1936; 35(1): 53–56.

[7] Korchevskii EM, Marochnik LS. Magnetohydrodynamic version of movement of blood. *Biophysics*. 1965; 10: 411–413.

[8] Bakhti H, Azrar L. Steady flow of couple-stress fluid in constricted tapered artery: Effects of transverse magnetic field, moving catheter, and slip velocity. *Journal of Applied Mathematics*. 2016; 2016: 9289684. Available from: https://doi.org/10.1155/2016/9289684.

[9] Freeman NE. The effect of temperature on the rate of blood flow in the normal and in the sympathectomized hand. *American Journal of Physiology*. 1935; 113(2): 384–398.

[10] Adams T, Spielman WS, Holmes KR, Heisey SR, Chen MM. Proposed methods for the measurement of regional renal blood flow using heat transfer analysis. *Annals of Biomedical Engineering*. 1985; 13: 237–258. Available from: https://doi.org/10.1007/BF02584242.

[11] Chinyoka T, Makinde OD. Computational dynamics of arterial blood flow in the presence of a magnetic field and thermal radiation therapy. *Advances in Mathematical Physics*. 2014; 2014: 174–177. Available from: https://doi.org/10.1155/2014/915640.

[12] Sinha A, Misra JC, Shit GC. Effect of heat transfer on unsteady MHD flow of blood in a permeable vessel in the presence of non-uniform heat source. *Alexandria Engineering Journal*. 2016; 55(3): 2023–2033. Available from: https://doi.org/10.1016/j.aej.2016.07.010.

[13] Kumar D, Satyanarayana B, Kumar R, Kumar S, Deo N. Application of heat source and chemical reaction in MHD blood flow through permeable bifurcated arteries with inclined magnetic field in tumour treatments. *Results in Applied Mathematics*. 2021; 10: 100151. Available from: https://doi.org/10.1016/j.rinam.2021.100151.

[14] Dhairiyasamy R, Gabiriel D, Bunpheng W, Kit CC. Impact of silver nanofluid modifications on heat pipe thermal performance. *Journal of Thermal Analysis and Calorimetry*. 2025; 150: 2079–2098. Available from: https://doi.org/10.1007/s10973-024-13836-8.

[15] Devi SPA, Devi SSU. Numerical investigation of hydromagnetic hybrid Cu-Al_2O_3/water nanofluid flow over a permeable stretching sheet with suction. *International Journal of Nonlinear Sciences and Numerical Simulation*. 2016; 17(5): 249–257. Available from: https://doi.org/10.1515/ijnsns-2016-0037.

[16] Suresh S, Venkitaraj K, Selvakumar P, Chandrasekar M. Effect of Al_2O_3-Cu/water hybrid nanofluid in heat transfer. *Experimental Thermal and Fluid Science*. 2012; 38: 54–60. Available from: https://doi.org/10.1016/j.expthermflusci.2011.11.007.

[17] Takabi B, Shokouhm H. Effects of Al_2O_3-Cu/water hybrid nanofluid on heat transfer and flow characteristics in turbulent regime. *International Journal of Modern Physics C*. 2015; 26(4): 1550047. Available from: https://doi.org/10.1142/S0129183115500473.

[18] Jamshed W, Nisar KS, Ibrahim RW, Shahzad F, Eid MR. Thermal expansion optimization in solar aircraft using tangent hyperbolic hybrid nanofluid: A solar thermal application. *Journal of Materials Research and Technology*. 2021; 14: 985–1006. Available from: https://doi.org/10.1016/j.jmrt.2021.06.031.

[19] Hussain A, Hassan A, Al Mdallal Q, Ahmad H, Rehman A, Altanji M, et al. Heat transport investigation of magneto-hydrodynamics (SWCNT-MWCNT) hybrid nanofluid under the thermal radiation regime. *Case Studies in Thermal Engineering*. 2021; 27: 101244. Available from: https://doi.org/10.1016/j.csite.2021.101244.

[20] Waqas H, Muhammad T, Noreen S, Farooq U, Alghamdi M. Cattaneo-Christov heat flux and entropy generation on hybrid nanofluid flow in a nozzle of rocket engine with melting heat transfer. *Case Studies in Thermal Engineering*. 2021; 28: 101504. Available from: https://doi.org/10.1016/j.csite.2021.101504.

[21] Ghadikolaei SS, Hosseinzadeh K, Ganji DD, Jafari B. Nonlinear thermal radiation effect on magneto Casson nanofluid flow with Joule heating effect over an inclined porous stretching sheet. *Case Studies in Thermal Engineering*. 2018; 12: 176–187. Available from: https://doi.org/10.1016/j.csite.2018.04.009.

[22] Pak BC, Cho YI. Hydrodynamic and heat transfer study of dispersed fluids with submicron metallic oxide particles. *Experimental Heat Transfer*. 1998; 11(2): 151–170. Available from: https://doi.org/10.1080/08916159808946559.

[23] Suresh S, Venkitaraj KP, Selvakumar P, Chandrasekar M. Synthesis of Al_2O_3-Cu/water hybrid nanofluids using two step method and its thermo physical properties. *Colloids and Surfaces A: Physicochemical and Engineering Aspects*. 2011; 388(1–3): 41–48. Available from: https://doi.org/10.1016/j.colsurfa.2011.08.005.

[24] Mehryan SAM, Kashkooli FM, Ghalambaz M, Chamkha AJ. Free convection of hybrid Al_2O_3-Cu water nanofluid in a differentially heated porous cavity. *Advanced Powder Technology*. 2017; 28(9): 2295–2305. Available from: https://doi.org/10.1016/j.apt.2017.06.011.

[25] Alsagri AS, Nasir S, Gul T, Islam S, Nisar KS, Shah Z, et al. MHD thin film flow and thermal analysis of blood with CNTs nanofluid. *Coatings*. 2019; 9(3): 175. Available from: https://doi.org/10.3390/coatings9030175.

[26] Mondal D, Pandey AK, Das A. Flow and heat transfer analysis of an ionanofluid above a rotating disk undergoing torsion. *Chinese Journal of Physics*. 2025; 93: 127–157. Available from: https://doi.org/10.1016/j.cjph.2024.11.024.

[27] Mondal D, Das A, Pandey AK. Existence and nonuniqueness of solutions for flow driven by a revolving hybrid nanofluid above a stationary disk. *Journal of Mathematical Analysis and Applications*. 2025; 552(2): 129743. Available from: https://doi.org/10.1016/j.jmaa.2025.129743.

[28] Turkyilmazoglu M, Alotaibi A. On the viscous flow through a porous-walled pipe: Asymptotic MHD effects. *Microfluidics and Nanofluidics*. 2025; 29(6): 33. Available from: https://doi.org/10.1007/s10404-025-02808-5.

[29] Turkyilmazoglu M. Evidence of sheet-triggered nonlinear similarity flows during stretching and moving: Atomization and electrospinning with/without air resistance. *International Journal of Numerical Methods for Heat and Fluid Flow*. 2024; 34(9): 3598–3614. Available from: https://doi.org/10.1108/HFF-04-2024-0254.

[30] Kumar V, Sharma PL, Bains D. Thermal convection in a Brinkman porous medium saturated with couple-stress nanofluid: A Galerkin weighted residual approach for different conducting boundaries. *Rakenteiden Mekaniikka*. 2025; 58(1): 16–32. Available from: https://doi.org/10.23998/rm.149371.

[31] Sudarmozhi K, Sreelatha Devi V, Öztop HF, Ahmad H, Abd-Elmonem A, Jamshed W, et al. AI-neural network modelling of Williamson blood flow in porous medium Soret-Dufour effects with tetra hybrid nanoparticles. *International Communications in Heat and Mass Transfer*. 2026; 171: 110107. Available from: https://doi.org/10.1016/j.icheatmasstransfer.2025.110107.

[32] Rehman A, Sudarmozhi K, Ali Z, Pamucar D, Khan D, Saad AA. Mathematical simulation for influence of thermocapillary radiative MHD unsteady couple stress ternary hybrid nanofluid on stretching parallel surface. *Contemporary Mathematics*. 2025; 6(6): 7636–7653. Available from: https://doi.org/10.37256/cm.6620257996.

[33] Ahmad H, Ghazwani HA, Elsaeedy HI, Mosallem MM, Hayat AU. Numerical algorithm of fourth-grade nanofluid flow with heat transfer consists of aluminum alloys over a Riga plate. *Journal of Thermal Analysis and Calorimetry*. 2025; 150: 15723–15736. Available from: https://doi.org/10.1007/s10973-025-14713-8.

[34] Kapustenko PO, Arsenyeva OP, Varbanov PS, Tovazhnyanskyy LL. Heat transfer intensification in compact heat exchangers with channels of various geometries and size. *International Communications in Heat and Mass Transfer*. 2025; 167: 109273. Available from: https://doi.org/10.1016/j.icheatmasstransfer.2025.109273.

[35] Szűcs H. Numerical study to investigate the thermal characteristic length with coupled CFD-FEM simulations. *International Journal of Heat and Fluid Flow*. 2024; 106: 109312. Available from: https://doi.org/10.1016/j.ijheatfluidflow.2024.109312.

[36] Orosz Á, How BS, Yeo LS, Turunawarasu D, Andiappan V, Pimentel J, et al. Exhaustive enumeration of heat exchanger networks with minimum utility consumption using graph-theoretic approach. *Energy*. 2025; 335: 137898. Available from: https://doi.org/10.1016/j.energy.2025.137898.

[37] Kovács G, Kocsis Szürke S, Fischer S. Investigation of convective and radiative heat transfer of 21700 lithium-ion battery cells. *Batteries*. 2025; 11(7): 246. Available from: https://doi.org/10.3390/batteries11070246.

[38] Morauszki T, Mándli P, Horváth Z, Dreyer MR. Simulation of fluid flow, combustion and heat transfer processes in internal combustion engines. *Hungarian Journal of Industrial Chemistry*. 2011; 39(1): 27–30. Available from: https://doi.org/10.1515/377.

[39] Szűcs H. Exploring the impact of compressibility on reconstructed porous materials: A numerical study. *Journal of Engineering Research*. 2025; 13(3): 1987–2003. Available from: https://doi.org/10.1016/j.jer.2024.07.018.

[40] Orosz Á, Friedler F. Multiple-solution heat exchanger network synthesis for enabling the best industrial implementation. *Energy*. 2020; 208: 118330. Available from: https://doi.org/10.1016/j.energy.2020.118330.
[41] Liao SJ. *Homotopy Analysis Method in Nonlinear Differential Equations*. Berlin: Springer; 2012.
[42] Liao S. *Beyond Perturbation: Introduction to the Homotopy Analysis Method*. Boca Raton, FL: Chapman and Hall/CRC; 2003.
[43] Liao S. An optimal homotopy-analysis approach for strongly nonlinear differential equations. *Communications in Nonlinear Science and Numerical Simulation*. 2010; 15(8): 2003–2016. Available from: https://doi.org/10.1016/j.cnsns.2009.09.002.
[44] Liao S. On the homotopy analysis method for nonlinear problems. *Applied Mathematics and Computation*. 2004; 147(2): 499–513. Available from: https://doi.org/10.1016/S0096-3003(02)00790-7.
[45] Sulochana C, Shivapuji GC. Numerical analysis of hybrid nanofluid flow over a nonlinear stretching sheet with viscous dissipation, Joule heating effects. *CFD Letters*. 2022; 14(10): 42–55. Available from: https://doi.org/10.37934/cfdl.14.10.4255.